power density, and angular position of the specimen were determined from this study. The most important finding in our study is that the water protects the recording x-ray resist from debris.

8. There are some reports of imaging hydrated specimens with laser pulses of several tens of joules of energy. To our knowledge, there was only one report of observing specimen in water with a laser plasma [R. W. Eason, M. Clague, R. Cherry, *Annual Report* (Rutherford Appleton Laboratory, Didcot, United Kingdom, 1985), p. A4.2.5] They used 30- to 40-J, 1-ns laser pulses. R. A. Cotton *et al.* (paper presented at the International Conference on X-Ray Microscopy, King's College, London, September 1990) reported that their x-ray flux produced by a 0.5-J, 25-ns laser pulse was sufficient for imaging dehydrated specimens but insufficient for hydrated specimens.
9. R. J. Rosser *et al.*, *Appl. Opt.* **26**, 4313 (1987).
10. The x-ray from our laser plasma showed a broad spectrum peaked at 2.8 nm. The water thickness in the experiment was estimated to be 3 μm from the transmission through the specimen. By taking account of the spectral dependence of the transmission through the 0.1-μm $Si_3N_4$ membrane and 3 μm of water and the sensitivity of the PMMA resist, the spectrum effective to the resist exposure was calculated. The main contribution comes from the x-rays of 2.4- to 3.0-nm wavelength. The contribution of x-rays outside the water-window region is negligibly small.
11. G. Giudice, Ed., *The Sea Urchin Embryo* (Springer-Verlag, Berlin, 1987), pp. 23–29.
12. When the dissolution rate $R$ of a resist has a relation with the x-ray dose $E$ of $R \propto E^n$, the relief height $h$ is given by $h = (1 - T^n)d$, where $T$ is the transmission of the specimen and $d$ is the developed resist depth. The integrated density of the specimen can be calculated from the transmission and the absorption coefficient.
13. Living cells are mainly composed of proteins, lipids, and water. In proteins and lipids, the density of carbon is roughly 0.7 g/cm$^3$ from the data in (*16*). Nitrogen contained in protein contributes an additional 10% to the absorption.
14. A flagellum consists of the so-called axoneme and a ciliary membrane. The axoneme is made of nine outer microtubule doublets and two central microtubules. Outer doublets are arranged in a circle and connected to the center tubules by radial spokes. Periodicity of 0.2 to 0.4 μm is not known in this structure. R. D. Allen [*J. Cell. Biol.* **37**, 825 (1968)] reported EM images of transverse section through flagella of a unicellular organism *Tetrahymena*. In his pictures, the shape of the ciliary membrane is irregular and shows the flexibility of the ciliary membrane. Flagella of various species are considered to have the similar structure.
15. C. Jacobsen *et al.*, in *X-ray Microscopy II*, D. Sayre, M. Howells, J. Kirz, H. Rarback, Eds. (Springer-Verlag, Berlin, 1988), pp. 253–262.
16. R. A. London, M. D. Rosen, J. E. Trebes, *Appl. Opt.* **28**, 3397 (1989).
17. According to (*16*), the maximum allowable exposure time for 0.03-μm resolution is 27 ps when the x-ray dose is 15 kJ/g and the ratio of specific heats $\gamma$ is 1.1. In our experiment, x-ray flux was 5 to 10 mJ/cm$^2$ and the x-ray dose in the sperm was 100 to 200 J/g. For the 500-ps duration x-ray exposure, the resolution is calculated to be ~0.06 μm.
18. The authors thank M. Morisawa of Misaki Marine Biological Station of the Tokyo University for providing the sea urchin, and Seiko Instruments, Inc., for the measurement by AFM.

19 November 1990; accepted 6 February 1991

---

# Atmospheric Lifetime of $CHF_2Br$, a Proposed Substitute for Halons

R. TALUKDAR, A. MELLOUKI, T. GIERCZAK,* J. B. BURKHOLDER, S. A. MCKEEN, A. R. RAVISHANKARA†

**The rate coefficients, $k_1$, for the reaction of OH with $CHF_2Br$ have been measured using pulsed photolysis and discharge flow techniques at temperatures ($T$) between 233 and 432 K to be $k_1 = (7.4 \pm 1.6) \times 10^{-13} \exp[-(1300 \pm 100)/T]$ cubic centimeters per molecule per second. The ultraviolet absorption cross sections, $\sigma$, of this molecule between 190 and 280 nanometers were measured at 296 K. The $k_1$ and $\sigma$ values were used in a one-dimensional model to obtain an atmospheric lifetime of approximately 7 years for $CHF_2Br$. This lifetime is shorter by approximately factors of 10 and 2 than those for $CF_3Br$ and $CF_2ClBr$, respectively. The ozone depletion potentials of the three compounds will reflect these lifetimes.**

SINCE THE SIGNING OF THE MONTREAL protocol (*1*) curtailing, and eventually banning, the production of chemicals that can destroy stratospheric ozone, many new compounds have been proposed as substitutes for the regulated compounds. Bromocarbons (Halons), for example, $CF_3Br$, and $CF_2ClBr$, which are used as fire-extinguishing agents, are major anthropogenic sources of stratospheric Br and will have to be replaced (*1*). One proposed substitute, $CHF_2Br$ (*2*), has good fire-suppression characteristics (*3*). This molecule, because of the presence of an H atom, reacts with OH free radicals in the troposphere; as a result, the quantity of this molecule transported to the stratosphere is reduced. To judge the acceptability of this replacement, it is necessary to know the fraction of $CHF_2Br$ released at the earth's surface that will reach the stratosphere. A measure of this quantity is the tropospheric lifetime of the compound. Two processes that can destroy this molecule in the troposphere and thus reduce its transport to the stratosphere are (i) the reaction with the OH free radical

$$OH + CHF_2Br \rightarrow CF_2Br + H_2O;\ k_1 \tag{1}$$

and (ii) photolysis. The latter process is quantified by measurement of the absorption cross section, $\sigma$, in the ultraviolet (UV) region. We have measured the rates of these two processes and calculated the tropospheric lifetime.

We measured the rate coefficient, $k_1$, using two complimentary techniques: (i) discharge flow with laser magnetic resonance detection (DF-LMR) of OH and (ii) pulsed laser photolysis with laser-induced fluorescence detection (PP-LIF) of OH [see (*4, 5*)]. The experimental conditions used to measure $k_1$ are listed in Table 1. In the pulsed photolysis experiments, HONO was used as the OH precursor. Because $CHF_2Br$ is nearly transparent at 355 nm ($\sigma < 10^{-24}$ cm$^2$), the wavelength at which HONO was photolyzed, secondary reactions of $CHF_2Br$ photofragments were minimized. The mass flow rates of all compounds flowing through the reactor were measured with calibrated mass flowmeters, and the flow rates were then used to determine the concentration of $CHF_2Br$. The sample of $CHF_2Br$ had an analyzed purity of 98.8%; $CF_2ClBr$ (1%) and $CF_2HCl$ (0.2%) were the main impurities. We also analyzed the sample for the possible presence of $Br_2$ and HBr, which react very rapidly with OH, using UV and infrared (IR) spectral measurements and found them to be less than 1 ppm by volume each.

Secondary reactions of OH were negligible, as reported in earlier papers dealing with the OH reaction rate coefficient measurements (*4, 5*), under our experimental conditions (see Table 1). There was good agreement between data obtained by two independent methods. We are confident that our measurements do not have any large systematic errors. In the DF-LMR study, we could not measure $k_1$ below 268 K because $CHF_2Br$ sticks on the walls of the reactor.

The measured values of $k_1$ (Table 1 and Fig. 1) can be expressed in the Arrhenius form as

$$k_1 = (7.4 \pm 1.6) \times 10^{-13} \exp[-(1300 \pm 100)/T] \text{ cm}^3 \text{ molecule}^{-1} \text{ s}^{-1} \tag{2}$$

for temperatures ($T$) between 233 and 352 K. Even though $k_1$ was measured up to 432 K, data at $T > 352$ K are not included in the fit because of the slight curvature in the Arrhenius plot at the higher temperatures and because we use measurements made at

National Oceanic and Atmospheric Administration (NOAA), Aeronomy Laboratory, R/E/AL2, 325 Broadway, Boulder, CO 80303, and The Cooperative Institute for Research in Environmental Sciences, University of Colorado, Boulder, CO 80309.

---

*On leave from the Department of Chemistry, Warsaw University, Zwirki i Wigury 101, 02-089 Warsaw, Poland.

†To whom correspondence should be addressed at NOAA. Also affiliated with the Department of Chemistry and Biochemistry, University of Colorado, Boulder, CO 80309.

atmospheric temperatures for lifetime calculations. The contributions of the reactions of OH with the known impurities, $CF_2ClBr$ and $CHF_2Cl$, to the measured value of $k_1$ are negligible (<1%), on the basis of known rate coefficients for these reactions (*5, 6*). We believe, on the basis of the linear Arrhenius plot of $k_1$ at the lower temperatures and the chemical analyses of the $CHF_2Br$ sample, that contributions to the measured value of $k_1$ from impurity reactions are negligible.

We measured the UV absorption cross sections of $CHF_2Br$ at 296 K using a $D_2$ lamp-diode array spectrometer (7). The measured $\sigma$ values were corrected for the contribution from $CF_2ClBr$ impurity (1%) in our sample. The obtained UV absorption spectrum is displayed in Fig. 2. The uncertainty in the $\sigma$ value at 280 nm is ~40%, and it increases rapidly at longer wavelengths. This effect is attributed to the uncertainty in subtracting the contribution of the $CF_2ClBr$ impurity. Therefore, we have not reported $\sigma$ above 280 nm. We assume that light absorption by $CHF_2Br$ leads to dissociation.

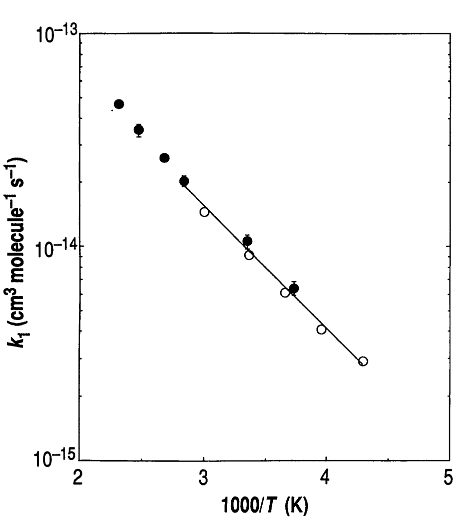

**Fig. 1.** Plot of $k_1$ (on a logarithmic scale) against the reciprocal of temperature. The closed circles are data obtained with the DF-LMR apparatus; the open circles are from the PP-LIF system. The line is a fit of the data obtained between 233 and 352 K to an Arrhenius relation; the parameters are given in Eq. 2.

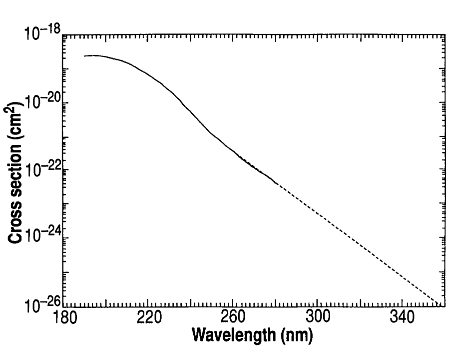

**Fig. 2.** UV absorption cross section $\sigma$ (on a logarithmic scale) plotted against wavelength $\lambda$ for $CHF_2Br$ at 296 K. The curve for $\lambda$ >280 nm (dashed line) was obtained by an extrapolation of the data measured between 260 and 280 nm and an assumption of an exponential decrease in $\sigma$ with $\lambda$.

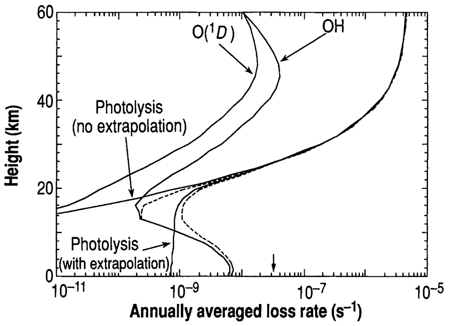

**Fig. 3.** Plot of the annually averaged loss rate of $CHF_2Br$ due to reaction with OH, $O(^1D)$, photolysis, and the sum of the three (dashed lines) as a function of altitude. "Photolysis (no extrapolation)" refers to the use of cross section with $\lambda$ <280 nm. "Photolysis (with extrapolation)" refers to the case when $\lambda$ up to 360 nm is used (see text). The downward-pointing arrow indicates a lifetime of 1 year.

**Table 1.** Summary of experimental conditions and the measured values of $k_1$ as a function of temperature. DF-LMR: The source of OH was the reaction of H with $NO_2$. PP-LIF: The source of OH was the 355-nm laser photolysis of HONO. Quoted error bars are $2\sigma$ and do not include estimated systematic errors.

| Temperature (K) | Method | $[OH]_o$ ($10^{10}$ $cm^{-3}$) | $[CHF_2Br]$ range ($10^{15}$ $cm^{-3}$) | Flow velocity ($cm\ s^{-1}$) | Buffer gas, pressure (torr) | $k_1$ ($10^{-14}$ $cm^3$ $molecule^{-1}$ $s^{-1}$) |
|---|---|---|---|---|---|---|
| 233 | PP-LIF | 42 to 84 | 37 to 314 | | He,100 | 0.29 ± 0.01 |
| 253 | PP-LIF | 94 | 55 to 325 | | He,100 | 0.41 ± 0.01 |
| 268 | DF-LMR | 0.7 to 8.8 | 1.03 to 7.74 | 850 | He,2 | 0.64 ± 0.05 |
| 273 | PP-LIF | 105 | 42 to 300 | | He,100 | 0.61 ± 0.01 |
| 297 | PP-LIF | 70 | 46 to 452 | | He,100 | 0.91 ± 0.01 |
| 298 | DF-LMR | 2.4 to 13.8 | 0.6 to 8.45 | 900 to 1200 | He,1 to 3 | 1.06 ± 0.08 |
| 333 | PP-LIF | 84 | 27 to 255 | | He,100 | 1.45 ± 0.04 |
| 352 | DF-LMR | 4.1 | 0.62 to 32.9 | 1050 | He,2 | 2.03 ± 0.12 |
| 373 | DF-LMR | 5.45 | 0.52 to 3.47 | 1500 | He,2 | 2.62 ± 0.08 |
| 405 | DF-LMR | 4.24 | 0.87 to 3.08 | 1700 | He,2 | 3.52 ± 0.23 |
| 432 | DF-LMR | 3.83 | 0.43 to 2.98 | 1800 | He,2 | 4.65 ± 0.17 |

Atmospheric lifetimes are usually calculated by two-dimensional (2-D) models (*8, 9*) or 3-D models (*10*). Our interest here is to calculate the lifetime of $CHF_2Br$ relative to those of existing Halons within a consistent modeling framework. To gauge the relative impact of two compounds on the atmosphere, at least to a first approximation, 1-D calculations are adequate. Therefore, we carried out 1-D calculations to measure the impact of substituting $CHF_2Br$ for $CF_2ClBr$ and $CF_3Br$. The OH rate constant and the UV absorption data were incorporated in a 1-D photochemical model to estimate the lifetimes of $CHF_2Br$ in the troposphere and the atmosphere (*5*, 7). Such a model has produced atmospheric lifetimes for chlorofluorocarbon replacements (7) that agree with 2-D models. A value of $1.0 \times 10^{-10}$ $cm^3$ $molecule^{-1}$ $s^{-1}$ for the rate constant for the reaction of $O(^1D)$ with $CHF_2Br$ was used. The contributions of the various processes to the rate of destruction of $CHF_2Br$ as a function of altitude are given in Fig. 3. The $O(^1D)$ reaction contributes negligibly to the loss of $CHF_2Br$ in the stratosphere and hence can easily be neglected. On the other hand, the contribution of photolysis to the calculated lifetimes is not negligible. Absorptions up to 360 nm contribute to this removal process. Even though the $\sigma$ values were not measured up to 360 nm, we estimate them by extrapolation of the measured shorter wavelength data between 260 and 280 nm. This extrapolation yields higher $\sigma$ values than that obtained by extrapolating the $\sigma$ values measured below 260 nm. We used the extrapolation made from 260 to 280 nm to ascertain the shortest possible lifetime. The calculated tropospheric and atmospheric lifetimes are 6.7 and 6.4 years, respectively. The tropospheric lifetime is 8 years if photolysis at a wavelength ($\lambda$) of >280 nm is neglected. Inclusion of longer wavelength (280 < $\lambda$ < 360 nm) photolysis makes the most difference between 8 and 20 km. Above 20 km, short-wavelength ($\lambda$ <280 nm) photolysis is the dominant loss process and inclusion of absorptions from 280 to 360 nm has minimal effect (Fig. 3). Photolysis (including contributions up to 360 nm) contributes at most 20% to the tropospheric lifetime. The UV cross sections in the tails of the absorption bands decrease with decreasing temperature (*5*). The same should be true for $CHF_2Br$. If the temperature dependence of $\sigma$ is included, the lifetime will increase. Therefore, we believe that the tropospheric lifetime of $CHF_2Br$ is between 6.7 years (obtained for temperature-independent cross sections up to a $\lambda$ of 360 nm) and 8 years (obtained by neglecting photolysis) while the atmospheric lifetime is approximately 7 years. The 7-year atmospheric lifetime of $CHF_2Br$ is shorter than the 12- to 18-year lifetime for $CF_2ClBr$ (*7, 11*) and the 65- to 81-year lifetime for $CF_3Br$ (*7, 11*). On a molecule per molecule basis, the improvement obtained by substituting $CHF_2Br$ for $CF_3Br$ is large. The same is not true for replacing $CF_2ClBr$. In the troposphere, $CHF_2Br$ is lost by reaction with OH, unlike $CF_2ClBr$ which is photolyzed. Determinations of lifetimes for species removed by OH reaction are reasonably well established, but tropospheric photolysis loss rates are not as well quantified.

---

REFERENCES AND NOTES

1. Montreal Protocol on Substances That Deplete the Ozone Layer (United Nations Environmental Programme, New York, 1987).
2. *Chem. Eng. News* **68** (no. 38), 34 (17 September 1990); *Chem. Week.* **146** (no. 21), 35 (30 May 1990).
3. R. S. Sheinson and D. C. Driscoll, paper presented at the 23rd International Symposium on Combustion, Orleans, France, 22–27 July 1990.
4. T. Gierczak, R. Talukdar, G. L. Vaghjiani, E. R. Lovejoy, A. R. Ravishankara, *J. Geophys. Res.* **96**, 5001 (1991).
5. J. B. Burkholder *et al.*, *ibid.*, p. 5025.
6. W. B. DeMore *et al.*, Chemical Kinetics and Photochemical Data for Use in Stratospheric Modeling (Evaluation No. 9, JPL Publication 90-1, Jet Propulsion Laboratory, Pasadena, CA, 1 January 1990).
7. J. J. Orlando, J. B. Burkholder, S. A. McKeen, A. R. Ravishankara, *J. Geophys. Res.* **96**, 5013 (1991).
8. D. A. Fisher *et al.*, *Nature* **344**, 508 (1990).
9. M. Prather and C. M. Spivakovsky, *J. Geophys. Res.* **95**, 18723 (1990).
10. R. G. Prinn and A. Golombek, *Nature* **344**, 47 (1990).
11. Global Ozone Research and Monitoring Project—Report 20, Scientific Assessment of Stratospheric Ozone (World Meteorological Organization, Geneva, 1989), vol. I, p. 430.

12. We thank R. Sheinson for providing the flame suppression data before publication and C. J. Howard for a critical reading of the manuscript. This research was carried out under the Radiatively Important Trace Species (RITS) component of the NOAA Climate and Global Change Program.

11 October 1990; accepted 19 February 1991

---

# Partial Melting of the Allende (CV3) Meteorite: Implications for Origins of Basaltic Meteorites

A. J. G. JUREWICZ, D. W. MITTLEFEHLDT, J. H. JONES

**Eucrites and angrites are distinct types of basaltic meteorites whose origins are poorly known. Experiments in which samples of the Allende (CV3) carbonaceous chondrite were partially melted indicate that partial melts can resemble either eucrites or angrites, depending only on the oxygen fugacity ($f_{O_2}$). Melts are eucritic if the $f_{O_2}$ is below that of the iron-wüstite buffer or angritic if above the $f_{O_2}$ of that buffer. With changing pressure, the graphite-oxygen redox reaction can produce oxygen fugacities that are above or below those of the iron-wüstite buffer. Therefore, a single, homogeneous, carbonaceous planetoid >110 kilometers in radius could produce melts of drastically different composition, depending on the depth of melting.**

EUCRITES AND ANGRITES ARE DISTINCT classes of basaltic meteorites. The initial Sr isotopic ratios from both groups, which are indistinguishable, indicate great age (*1, 2*). Similarly, their O isotopic compositions suggest derivation from the same isotopic reservoir (*3*), such as planetoids derived from adjacent regions of the solar nebula. Yet there are also radical differences between eucrites and angrites, as indicated by their respective mineralogies. Eucrites are composed mainly of Ca-poor clinopyroxene, anorthitic plagioclase, and tridymite (*4*), whereas angrites contain Ca-, Al-, and Ti-rich clinopyroxene, Ca-rich olivine, and anorthite (*5–7*) (Fig. 1). This difference in mineralogy is a reflection of different bulk compositions. For example, eucrites are silica-saturated, whereas angrites are critically silica-undersaturated. Because of the large difference in the degree of silica saturation between eucrites and angrites, they may be profitably thought of as analogs of terrestrial tholeiites and alkali basalts, respectively. Additionally, the Ca/Al ratios of the most primitive eucrites are close to those of chondritic meteorites, whereas the Ca/Al ratios of angrites are significantly higher (*8*). Eucrites are also thought to have formed under lower ambient oxygen fugacities ($f_{O_2}$) than did the angrites (*9–11*). Accordingly, explanations for the origins of these meteorites must take into account their basaltic textures, distinctive bulk compositions and mineralogies, similar Sr and O isotopic ratios, and different intrinsic $f_{O_2}$.

The origins of eucrites and angrites have been topics of considerable debate. The foci of these debates center around whether these meteorites are evolved melts, produced by complex fractional crystallization processes, or whether they are direct melts from undifferentiated nebular accretions, such as chondritic meteorites. For example, Mason (*12*), and more recently Hewins and Newsom (*13*), viewed eucrites as evolved basaltic liquids. If this hypothesis is correct, an initial, primitive liquid crystallized pyroxene and possibly minor olivine. The evolved, derivative liquid then separated from the accumulation of crystals and was quenched to form eucrites. In contrast, Stolper (*9*) provided evidence that at least some eucrites represent primary, undifferentiated liquids formed by direct melting. Stolper noted that eucrite compositions cluster about a low-pressure peritectic (reaction point) when plotted on a pseudo-ternary olivine-plagioclase-silica (OL-PL-SI) diagram. The compositions of chondritic meteorites can be approximated by this system, and the phase relations imply that peritectic melts of chondrites should be eucritic in composition. Debate over the merits of these end-member models continues.

The origin of angrites is even more obscure. Both complex and simple petrogeneses for angrites have been proposed [for example, (*8*) and references therein]. One suggestion is that angrites may be nebular condensates or slightly modified condensates (*14*). Such diversity of views reflects the strangeness of angrite mineralogies, as contrasted to the mineralogies of other igneous meteorites.

To gain insight into the petrogenesis of eucrites and angrites, we determined experimentally the compositions of low-pressure partial melts of the Allende (CV3) carbonaceous chondrite (*15*) and evaluated the effect of $f_{O_2}$ on melt composition. This meteorite was chosen for pragmatic reasons: representative samples are easily obtained, and the meteorite has been well characterized. Although Allende is not necessarily the best choice for specifically creating melts of either eucritic or angritic bulk composition, its composition (Table 1) was deemed reasonable for an initial assessment of direct melting models (*8*).

Experimental conditions were chosen to reflect inferred conditions of eucrite and angrite genesis. The temperature, 1200°C, was close to both the peritectic temperature of Stolper (*9*) and the liquidus temperature of the angrite LEW86010 (*16*). The $f_{O_2}$ was varied so that the most reducing $f_{O_2}$ was close to that inferred for eucrite genesis (*9*), whereas the higher $f_{O_2}$ values were close to those calculated for LEW86010 (*11*) and measured for Angra dos Reis (*10*). The $f_{O_2}$ values of our experiments bracketed the Fe-FeO (iron-wüstite) O buffer (IW): from one log unit below it (IW−1) to about two

---

A. J. G. Jurewicz and D. W. Mittlefehldt, Mail Code C23, Lockheed Engineering and Sciences Company, Houston, TX 77058.
J. H. Jones, SN2/Planetary Sciences Branch, National Aeronautics and Space Administration, Johnson Space Center, Houston, TX 77058.